Progress In Electromagnetics Research M, Vol. 111, 53–63, 2022

High-Isolation Wide-Beam Dual-Polarized Antenna Utilizing Symmetrical Feeding

Le Thi Cam Ha[1, 2], Son Xuat Ta[1, *], Nguyen X. Quyen[1], Nguyen K. Kiem, and Dao-Ngoc Chien[1]

Abstract—This paper presents a dual-polarized crossed-dipole antenna with high isolation and wide-beam radiation. The antenna comprises two orthogonal printed dipoles with single-ended and differential feeds, which are collocated on a square ground plane. The single-ended feed dipole is built on the peripheral sides of a two-layer substrate, and it is fed by a Γ-shaped stripline sandwiched between the substrate layers. The differential-feed dipole is built on a single-layer substrate, i.e., the differential feed with a Π-shaped microstrip-line, and the dipole arms are printed on the top-side and back-side of the substrate, respectively. The high isolation feature is achieved by exploiting the symmetry of the design with one pair of differential feeds. The beamwidth is significantly broadened by incorporating parasitic monopole elements while keeping the design symmetrical. A realization of the design concept for the 5G NR n78 band (3.3–3.8 GHz) has been optimized, fabricated, and tested. The measured results demonstrate an impedance bandwidth of 28.6% (3.0–4.0 GHz) and port-to-port isolation of > 40 dB. Furthermore, the antenna achieves a peak half-power beamwidth of 150°/168° in the E/H planes and a cross-polarization level of < -30 dB at the broadside direction. These features make the proposed antenna a good candidate for the 5G and in-band full-duplex applications.

1. INTRODUCTION

The fifth generation (5G) wireless communication networks with faster speeds and coverage are commercially deploying globally [1]. For the coverage regardless of place, besides outdoor base stations, a huge number of indoor access points are needed to be installed in obscured areas, such as inside buildings, underground complex, and subway stations [2]. Antennas are crucial components in the access points, which are designed to yield not only satisfying bandwidth but also proper radiation characteristics for the optimal coverage.

In indoor environment, wireless communication systems suffer from multiple reflections and scattering, which cause diversified polarization and multipath fading effects. Especially, under complex indoor scenarios, the single-polarization access points may not effectively transmit or receive the complex-polarized signals from the mobile terminals. To overcome this issue and improve the channel capacity, dual-polarized antennas [3] have been utilized as a powerful approach for the indoor wireless communications. Various dual-polarized antennas have been presented for the 5G indoor applications, such as patch antennas [4, 5], crossed dipoles backed by dielectric cavity [6], and aperture-couple-fed magneto-electric dipoles [7, 8]. Moreover, to achieve pervasive coverage, different techniques have been presented to widen the beamwidth of the dual-polarized antenna. The techniques, for instance, include adding parasitic elements [9], tetrahedral ground [10], cavity [11], notched wall [12], and via fence [13].

Received 2 May 2022, Accepted 1 June 2022, Scheduled 19 June 2022

* Corresponding author: Son Xuat Ta (xuat.tason@hust.edu.vn).

[1] School of Electrical and Electronic Engineering, Hanoi University of Science and Technology, Ha Noi 10000, Viet Nam. [2] Faculty of Engineering and Technology, Quy Nhon University, Quy Nhon, Viet Nam.

However, most of the above-mentioned dual-polarized antennas yield an isolation about 30 dB, which is not enough for some applications, e.g., in-band full-duplex (IBFD) communication [14].

IBFD technology has been one of the strongest candidates for the 5G and beyond 5G systems to address more stringent requirements, such as ultra-high data rate, energy efficiency, global coverage/connectivity, extremely high reliability, and low latency. In IBFD system, Tx and Rx signals use the same frequency simultaneously, and consequently, it benefits from potentially doubling the spectrum efficiency relative to the typical frequency/time-division duplex system. However, for this system to work, an IBFD antenna normally requires an isolation of > 40 dB between Tx and Rx, which is critically challenging [15].

The objective of this paper is to design a dual-polarized antenna with very high isolation and large beamwidth, which covers the 5G NR n78 bands from 3.3 to 3.8 GHz. The antenna will be a potential candidate for IBFD indoor wireless communication. All of the aforementioned requirements, including high isolation, large beamwidth, and large bandwidth, can make this design challenging. First, as mentioned before, typical dual-polarized antennas only achieve an isolation about 30 dB. Second, high isolation can be achieved with orthogonal polarization and double differential feeding [16–19]; however, it might not be simple to modify these structures for a wider beamwidth.

In this paper, we exploit the symmetry of a crossed-dipole to achieve a very high isolation with only one pair of differential feeds. The key design technique is to modify the feeding and the geometry of the dipoles such that the whole structure maintains a *plane of symmetry*. This ensures a theoretical isolation of infinity. The selected design structure also allows us to extend the beamwidth by adding parasitic elements. This feature is analytically explained in this paper.

2. ANTENNA DESIGN AND CHARACTERISTICS

2.1. Design Concept

Figure 1(a) shows a typical design of a printed dipole with a single-ended feed. The feeding structure is an integrated balun, which consists of a Γ-shaped microstrip-line coupled to a coplanar-stripline. This type has been widely utilized in several previous dual-polarized printed dipoles, e.g., see [11]. The unbalanced structure of the balun degrades the port-to-port isolation, and consequently, antennas

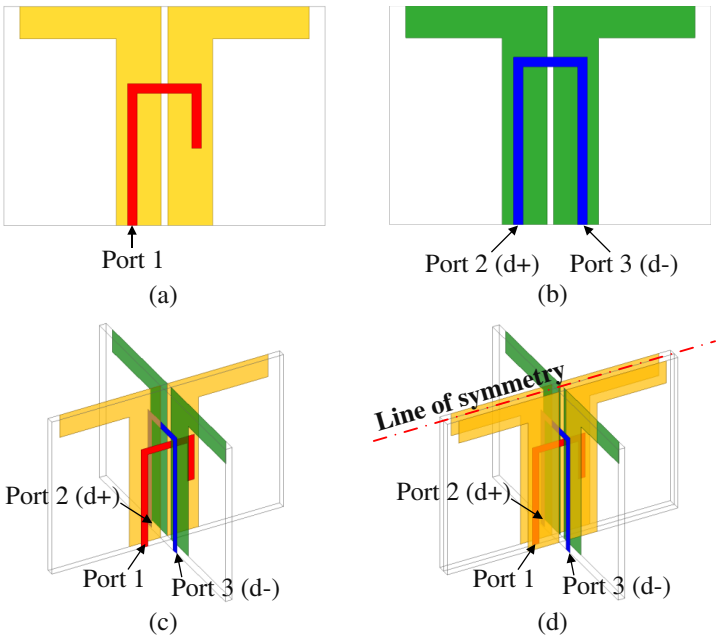

Figure 1. (a) Printed dipole with single-ended feed; (b) printed dipole with differential feed; (c) crossed-dipoles with single-ended and differential feeds; (d) design concept of the proposed antenna.

utilizing this feeding only achieved an isolation up to about 30 dB [9–11]. This is because when the other orthogonal dipole similar to Fig. 1(a) is added, the feed breaks the symmetry of the whole structure.

A printed dipole can be excited by a balanced structure of a differential-feed scheme, as shown in Fig. 1(b). Ports 2 and 3 are arranged symmetrically to excite two dipole arms with the same magnitude and out-of-phase (Fig. 1(c)). The reflection coefficient of the differential port, i.e., port d, is as:

$$S_{dd} = \frac{1}{2}\left(S_{22} - S_{23} - S_{32} + S_{33}\right). \tag{1}$$

The coupling between Port 1 and the differential port (Port d), S_{d1}, [20] is

$$S_{d1} = \frac{1}{\sqrt{2}}\left(S_{21} - S_{31}\right) \tag{2}$$

For high isolation, the requirement is $S_{21} = S_{31}$, which is satisfied as long as the structure is symmetrical across Port 2 and Port 3. Examining Fig. 1(c) closely, it can be observed that this structure is still not entirely symmetrical. This is because the feed of Port 1 (red line) is printed in one substrate layer, and the dipole is printed on the other substrate layer. Therefore, in the case of Fig. 1(c), S_{21} is not the same as S_{31}, which increases the coupling between the differential port and Port 1. In order to maintain a perfect symmetry, the design concept is shown in Fig. 1(d): The dipole at Port 1 is printed in both peripheral layers of a two-layer substrate, while the feed line is centered in the middle. In this case, the whole structure exhibits a plane of symmetry across Port 2 and Port 3, i.e., the vertical plane containing the symmetry line in Fig. 1(d). This will ensure that $S_{d1} = 0$ using (2).

2.2. Antenna Geometry

Using the proposed concept in Fig. 1(d), the antenna is realized as shown in Fig. 2. The antenna consists of two orthogonal printed dipoles (Dipole-1 and Dipole-2), which are collocated on a square ground plane. Dipole-1 uses a single-ended feeding structure, while Dipoles-2 is designed with a differential

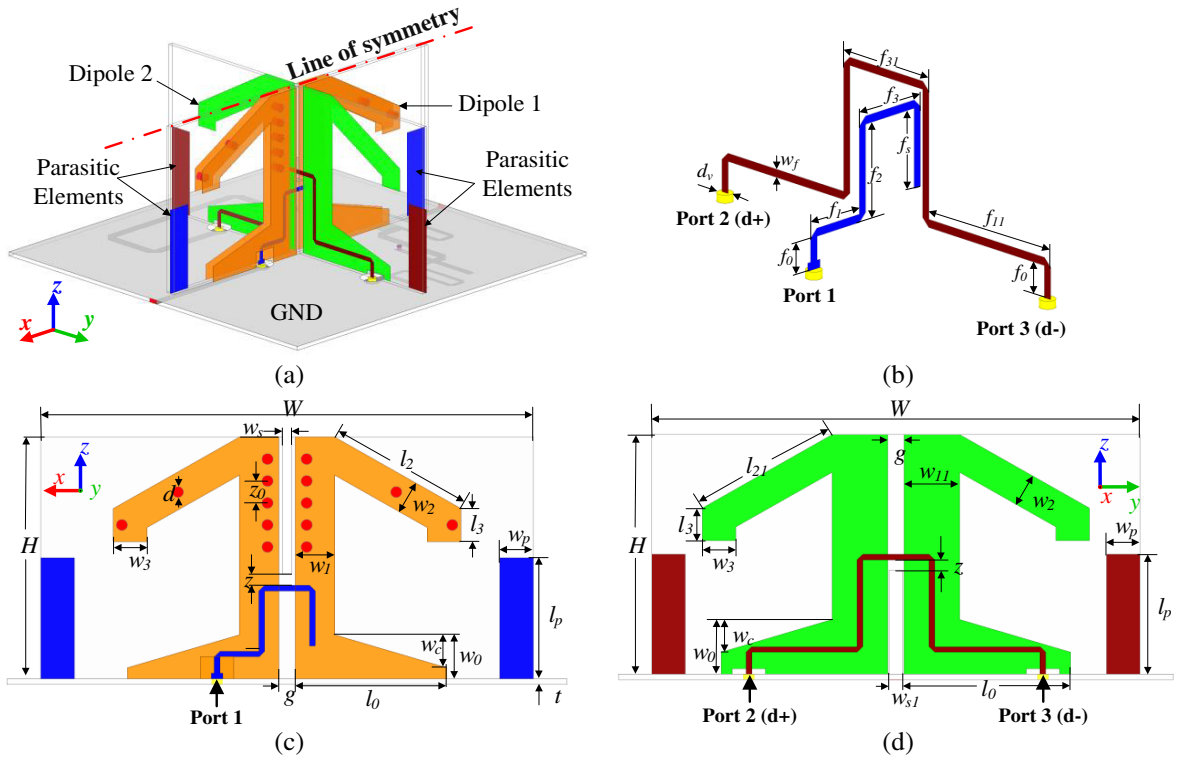

Figure 2. Geometry of the proposed antenna: (a) perspective view; (b) Γ-shaped strip-line and Π-shaped microstrip-line; (c) front-view of Dipole-1; (d) front-view of Dipole-2.

feed. Dipole-1 is built on the peripheral sides of a two-layer substrate and is fed by a Γ-shaped stripline sandwiched between the substrate layers. Its arms on different sides are shorted by vias to assist the attachment of two substrates. Dipole-2 is built on a single-layer substrate; its differential feed with a Π-shaped microstrip-line is printed on the top-side of the substrate, whereas its dipole arms are on the back-side of the substrate. All substrates are FR4 sheets ($\varepsilon_r = 4.4$ and $\tan\delta = 0.02$) with a 0.6-mm thickness for each layer. To broaden the beamwidth, parasitic elements of vertical strips are placed symmetrically at the side of the dipole. The proposed antenna is optimized for the 5G NR n78 band (3.3–3.8 GHz) with features of broadband, dual-polarization, high isolation, and wide-beam radiation pattern. The final design parameters are given in Table 1.

Table 1. Design parameters of the proposed antenna (unit: mm).

W_g	W	H	z	g	w_s	w_{s1}	d	l_0	w_0
50	44	22	3	1.5	0.8	1.3	1	10	5
w_c	w_1	l_2	w_2	l_3	w_3	w_{11}	l_{21}	l_p	w_p
3	3.5	12.8	3	3	3	4.7	13.2	12	3
f_0	f_1	f_{11}	f_2	f_3	f_{31}	f_s	w_f	d_v	z_0
2	2	10	6	7	7	5	0.5	1	2

2.3. Design Evolution

To assist in understanding the design procedure, the design evolution of the proposed antenna is illustrated in Fig. 3(a). The initial design (Ant. 1) is a conventional printed dipole with an integrated balun [21], which is vertically placed on a square ground plane of 50 × 50 mm^2. From the initial design, the printed dipole is modified with different feeding configurations of single-ended and differential schemes to establish Ant. 2 and Ant. 3, respectively. Finally, Ant. 2 and Ant. 3 employ parasitic elements of vertical strips to broaden the beamwidth. The two modified dipoles are optimized individually, and then they are orthogonally arranged on the ground plane to establish the final design.

Although the two dipoles employ differential feeds, their radiation mechanisms are similar to the conventional design [21], i.e., there are two resonances in their reflection coefficient profiles. The lower

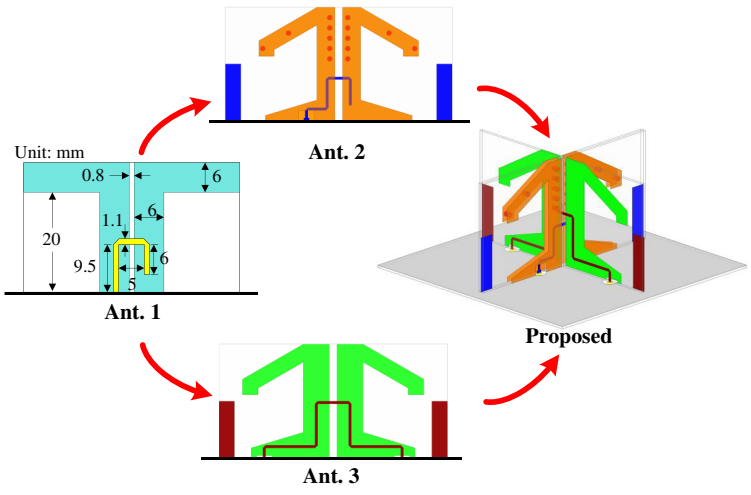

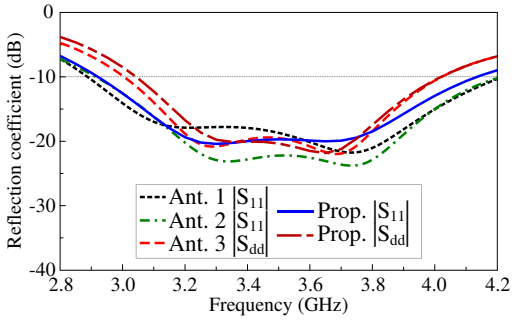

Figure 3. (a) Design evolution of the proposed antenna; (b) Reflection coefficients of the different antenna configurations.

resonance is mainly determined by the dipole length, while the upper one is mainly determined by the slot length from the integrated balun to the dipole. Therefore, the design parameters of Ants. 2 and 3 are similar to those of the proposed antenna. Fig. 3(b) shows the simulated reflection coefficients of all antennas. It is observed that these designs yield a broadband characteristic. Their impedance matching bandwidths completely cover the 5G NR n78 band (3.3–3.8 GHz).

Figure 4 shows the isolations of a conventional dual-polarized dipole and the proposed antenna. The conventional design, as shown in the left-inset of Fig. 4, consists of two Ant. 1 structures, which are orthogonally arranged on a square ground plane. As the structure of the conventional dual-polarized antenna is asymmetrical, its isolation is just about 30 dB. It can be observed from Fig. 4 that the simulated isolation for the proposed design is much higher. In fact, by ensuring the structural symmetry, the theoretical port-to-port isolation should be infinite (since $S_{d1} = 0$ as proved in (2)). The simulated value of about 60 dB (solid blue curve) in Fig. 4 is just due to the numerical error of full-wave numerical simulation. It is noted that in practice, the isolation of this symmetrical-designed structure is mainly affected by the quality of the feeding network, i.e., the 180° phase shifter and the tolerance in fabrication (see Section 3).

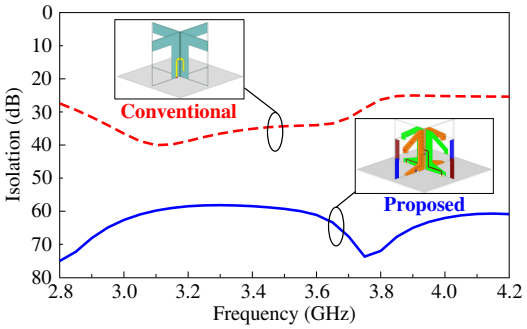

Figure 4. Isolation comparison of the proposed antenna and the conventional crossed dipoles.

2.4. Widebeam Radiation

For the indoor access points, the antenna normally requires a wide-beam radiation for the pervasive coverage. To address this issue, the proposed antenna employs parasitic elements of vertical strips to broaden the beamwidth [9]. To further understand the mechanism of beamwidth broadening, we aim to analytically estimate the radiation pattern with and without the parasitic elements. It is noted that this feature was only qualitatively explained in [9]. As illustrated using simulated surface current in Fig. 5(a), the antenna sources can be considered as three currents, I_1, $0.5I_2$, $-0.5I_2$, above the ground plane (Fig. 5(b)). Using image theory, the system is equivalent to a system of 4 currents as in Fig. 5(b) (shown in the right figure). The far-field electric field of this system of 4 currents can be estimated as

$$E_\theta(\theta) \propto I_1 \cos\theta e^{jkd_1 \cos\theta} - I_1 \cos\theta e^{-jkd_1 \cos\theta} + I_2 \sin\theta e^{jkd_1 \sin\theta} - I_2 \sin\theta e^{-jkd_1 \sin\theta} \tag{3}$$

where $0 \le \theta \le \pi/2$ (assuming a very large ground plane). Without the strips, the radiation pattern is estimated as

$$E_\theta(\theta) \propto I_1 \cos\theta e^{jkd_1 \cos\theta} - I_1 \cos\theta e^{-jkd_1 \cos\theta} \tag{4}$$

It is noted that Equations (3) and (4) assume that the lengths of the dipoles and strips are small. Although they are rough approximations, Equations (3) and (4) are still useful in predicting how the radiation patterns are modified with these strips.

To confirm the effects of the parasitic elements, the radiation patterns of Ants. 1 and 3 are theoretically calculated and simulated at 3.55 GHz and given in Fig. 5(c). It is noted that to obtain the calculated results in Fig. 6(c), we estimate $I_2 \approx 0.5I_1$ as the excitation of strips should have a smaller magnitude than the main dipole. A very good agreement between calculation and simulation verified the above analysis. The results indicate that the strips broaden the E-plane beamwidth of the printed dipole, i.e., Ant. 1 (without strips) yields a half-power beamwidth (HPBW) of 70°, while Ant. 3 (with

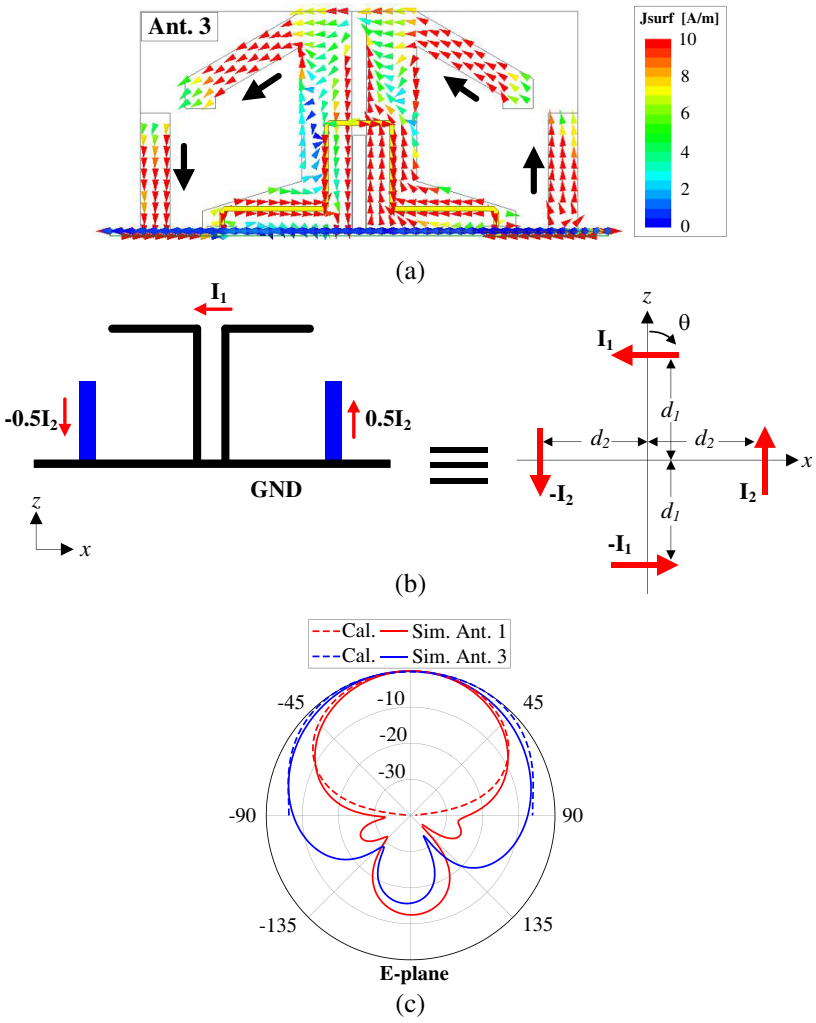

Figure 5. (a) Simulated surface current on Ant. 3 at 3.55 GHz, (b) principle of the widebeam radiation, (c) calculated and simulated 3.55-GHz radiation pattern of Ant. 1 and Ant. 3.

strips) achieves an HPBW of 120°. The effects of the strips on Ant. 2 are similar to Ant. 3, so they are not shown for brevity.

Using (3), it can be analytically predicted that the beamwidth is mainly affected by the magnitude of I_2 relatively to I_1, which can be controlled by changing the strip length l_p and distance d_2. This has been confirmed with full-wave numerical simulations. Thus, the distance between two parasitic elements and the lengths of strips are optimized to achieve the optimal beamwidth across the operating frequency range.

3. REALIZATION AND MEASUREMENTS

To realize the differential feed for the proposed antenna, a wideband out-of-phase power divider [22] is employed. The geometry of the differential feed is illustrated in Fig. 6(a), which includes a Wilkinson power divider and a wideband 180° phase shifter. The feeding network is built on a Roger RO4003 substrate ($\varepsilon_r = 3.38$, $\tan\delta = 0.02$, and thickness of 0.508 mm) and optimized for the 5G NR n78 band. Fig. 6(b) shows the simulated S-parameters and phase differences at outputs of the power divider. It yields $|S_{11}| < -20$ dB, $|S_{21}| = |S_{31}| = 3.5 \pm 0.1$ dB, and a phase difference of $180° \pm 1°$ at 3.0–4.0 GHz.

For verification, the proposed antenna is fabricated and measured. Its components, including printed dipoles and feeding network, are realized using printed circuit board technology. Fig. 7(a)

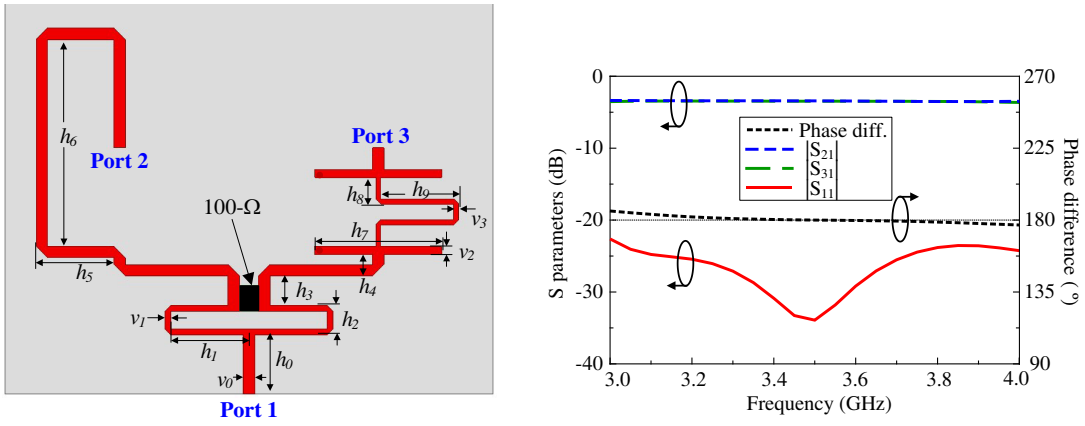

Figure 6. (a) out-of-phase power divider ($h_0 = 6$, $h_1 = 8$, $h_2 = 3$, $h_3 = 3$, $h_3 = 2.2$, $h_5 = 8$, $h_6 = 21$, $h_7 = 13$, $h_8 = 2.7$, $h_9 = 8$, $v_0 = 1.14$, $v_1 = 0.6$, $v_2 = 0.8$, $v_3 = 0.5$; unit: mm); (b) its S-parameters and phase difference at the outputs.

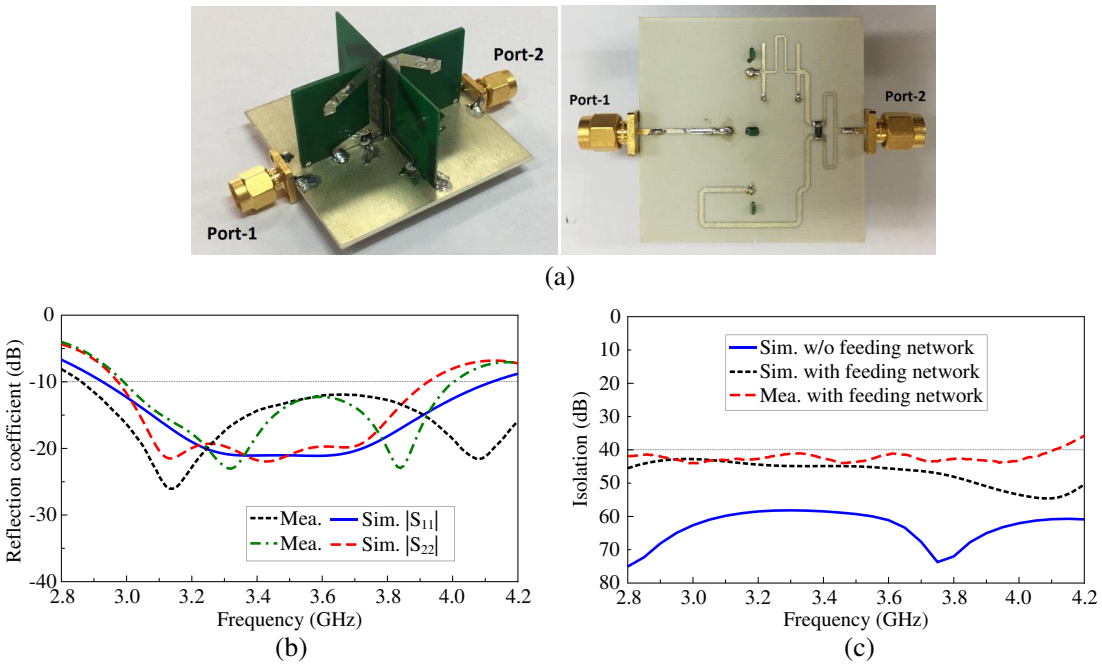

Figure 7. (a) A fabricated prototype of the proposed antenna; Simulation and measurement: (b) reflection coefficient and (c) isolation values.

shows the fabricated prototype. For a sturdy construction, several bumps and corresponding rabbets are added into the dipole substrates and the ground plane, respectively. The S-parameters of the prototype are measured by using a vector network analyzer. From Fig. 7(b), it is observed that the measured results agree quite closely with the simulations. The measurements result in a bandwidth of 28.6% (3.0–4.0 GHz) for −10-dB reflection coefficient. As shown in Fig. 7(c), the measured isolation of the prototype is worse than the theoretical value due to the imperfect feeding network and fabrication tolerance. Nevertheless, the measured port-to-port isolation is > 40 dB as compared to the simulated value of > 42.5 dB (with feeding network).

The radiation characteristics of the antenna prototype are measured in an anechoic chamber. Fig. 8

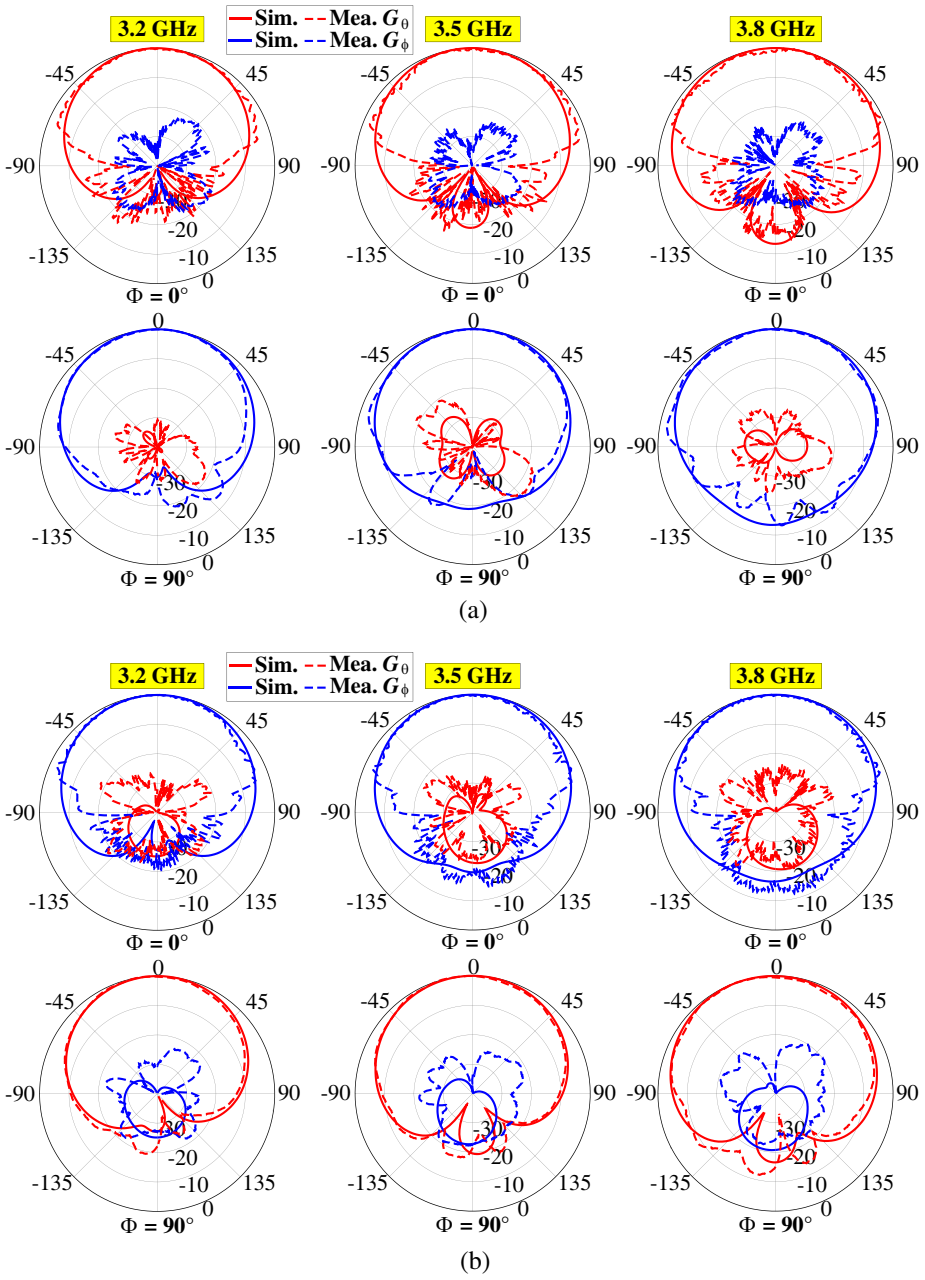

Figure 8. The radiation patterns of the proposed antenna: (a) Port 1 excitation and (b) Port 2 excitation.

illustrates the radiation patterns for Ports 1 and 2 excitations. The antenna achieves a stable radiation: symmetric profile, wide beamwidth, high front-to-back (F-B) ratio, and low cross-polarization. Due to the presence of the tapping and foam-racking in the measurement setup, the measured cross-polarizations are larger than the simulated values. Nevertheless, the cross-polarization is still $< -30\,\text{dB}$ at the broadside direction ($\theta = 0°$). Fig. 9 illustrates the realized gain and HPBWs of the antenna prototype. As frequency increases, the broadside gains decrease, which is accompanied by widening the beamwidths in both E and H planes. As shown in Fig. 9(a), the gain at Port 2 is slightly lower than Port 1, which is attributed to the losses caused by the feeding network. From Fig. 9(b), the antenna achieves the peak values of HPBW at 3.95 GHz, which are 150°/168° in the E/H planes, respectively.

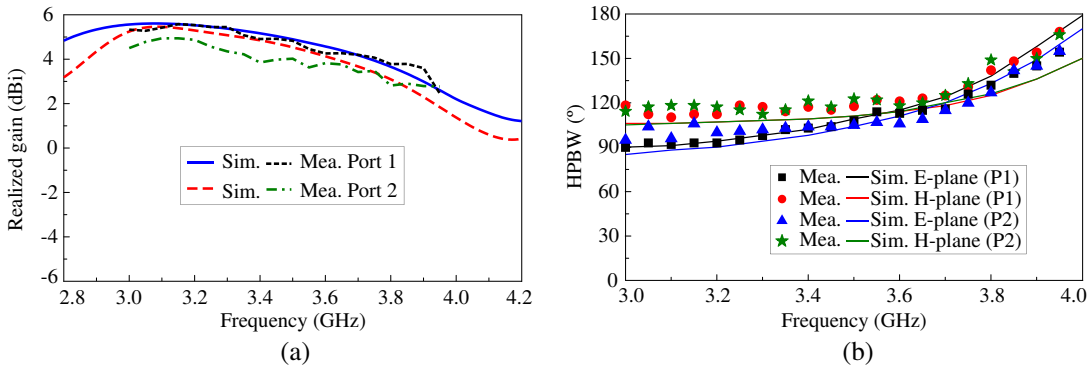

Figure 9. (a) Realized gain and (b) HPBWs of the proposed antenna.

4. PERFORMANCE COMPARISON AND DISCUSSION

A performance comparison between the proposed antenna and the related priors is given in Table 2. Firstly, as compared to most antennas with single-ended feed scheme [4–13], the proposed antenna yields a significantly higher isolation, comparable overall-size, and bandwidth. Secondly, the proposed

Table 2. Performance comparison between the proposed antenna and the related priors.

Ant.	Overall size (λ_{min})	Feed Scheme	BW (%)	Peak HPBW (°) in E/H planes	Isolation (dB)
[4]	0.79 × 0.79 × 0.062	Single-ended	5.7	74/74	25
[5]	0.47 × 0.64 × 0.122	Single-ended	25.0	Not mentioned	15
[6]	0.44 × 0.44 × 0.15	Single-ended	19.7	85/85	40
[7]	0.66 × 0.66 × 0.104	Single-ended	27.6	Not mentioned	28
[8]	0.50 × 0.50 × 0.125	Single-ended	33.0	75/75	25
[9]	0.54 × 0.54 × 0.15	Single-ended	25.0	92/110	28
[10]	0.7 × 0.7 × 0.37	Single-ended	22.6	83/90	31
[11]	0.53 × 0.53 × 0.24	Single-ended	60.0	76/80	25
[12]	0.74 × 0.74 × 0.19	Single-ended	13.3	90/85	20
[13]	1.4 × 1.4 × 0.125	Single-ended	33.0	107/105	32
[17]	0.66 × 0.66 × 0.123	Double differential	37.5	60/70	40
[18]	2.6 × 2.6 × 0.624	Double differential	17.5	100/100	50
[19]	1.05 × 1.05 × 0.115	Double differential	47.3	74/50	40
[20]	0.97 × 0.97 × 0.08	Single-ended and Differential	28.4	70/56	43.0
[23]	0.77 × 0.88 × 0.013	Single-ended and Differential	2.1	Not mentioned	62
[24]	1.23 × 1.38 × 0.01	Single-ended and Differential	103	Not mentioned	30.0
Prop.	**0.50 × 0.50 × 0.22**	**Single-ended and Differential**	**28.6**	**150/168**	**40**

antenna achieves a similar isolation, but a simpler feeding structure, related to the double differential-feed designs [17–19]. Finally, the proposed antenna achieves a widest HPBW relative to the priors.

Although the combination of a single-ended and a differential feeding structure has been used before, e.g., [20, 23, 24], there are still several key merits using the proposed design. First, the IBFD antenna [20] exploited the wideband and low-profile features of the metasurface to achieve an isolation of > 43 dB across 28.4% bandwidth at 3.5 GHz. The metasurface, however, needs a relatively large footprint for the wideband characteristic. Furthermore, it is challenging to achieve wide-beam radiation for this design. The patch antenna [23] is fed by a single-ended port as Tx and a differential feeding as Rx to achieve an isolation > 62 dB within only 2% bandwidth at 2.41 GHz. It is noted that achieving high isolation across a wide range of frequency is much more difficult. Finally, the monostatic printed monopole in [24] is fed by a single-ended port for Tx and a differential scheme realized by an out-of-phase power divider for Rx. However, the feeding structure is not perfectly symmetrical, which gives rise to mutual coupling, i.e., the isolation is only 30 dB. Overall, as compared to the dual-polarized antennas with similar feeding structures (single-ended and differential feeds), the proposed design yields a smaller footprint and a larger beamwidth in the trade-off of a higher profile.

5. CONCLUSION

A high-isolation dual-polarized antenna with wide-beam radiation has been described. The key concept is to modify the antenna and feeding structure such that perfect symmetry is maintained across the pair of differential ports. For realization, the design is constructed by two orthogonal printed dipoles where the single-ended feed dipole is built on peripheral sides of a two-layer substrate, and the differential-fed dipole is fed by a Π-shaped microstrip-line. To broaden the beamwidth, the printed dipoles are incorporated with parasitic elements. A fabricated prototype resulted in an impedance matching bandwidth of 28.6% (3.0–4.0 GHz) and port-to-port isolation of > 40 dB, peak beamwidth of $150^\circ/168^\circ$ in the E/H planes, and a cross-polarization level of < -30 dB at $\theta = 0^\circ$. With features of broadband, dual-polarization, high isolation, wide-beam, and high efficiency, the proposed antenna is a good candidate for the indoor 5G access points, and it can be found useful in different full-duplex wireless communication systems.

REFERENCES

1. Sag, A., "The state of 5G in early 2021, Pt. 2," Accessed May 02, 2022, [Online]. Available: https://www.forbes.com/sites/moorinsights/2021/03/16/the-state-of-5g-in-early-2021-pt-2/?sh=31a0a8875ad9.
2. Tonini, F., M. Fiorani, M. Furdek, C. Raffaelli, L. Wosinska, and P. Monti, "Radio and transport planning of centralized radio architectures in 5G indoor scenarios," *IEEE Journal on Selected Areas in Communications*, Vol. 35, No. 8, 1837–1848, Aug. 2017.
3. Mirmozafari, M., G. Zhang, C. Fulton, and R. J. Doviak, "Dual-polarization antennas with high isolation and polarization purity: A review and comparison of cross-coupling mechanisms," *IEEE Antennas Propagat. Mag.*, Vol. 61, No. 1, 50–63, Feb. 2019.
4. Huang, H., X. Li, and Y. Liu, "A low-profile, single-ended and dual-polarized patch antenna for 5G application," *IEEE Transactions on Antennas and Propagation*, Vol. 68, No. 5, 4048–4053, May 2020.
5. Xue, K., D. Yang, C. Guo, H. Zhai, H. Li, and Y. Zeng, "A dual-polarized filtering base-station antenna with compact size for 5G applications," *IEEE Transactions on Antennas and Propagation*, Vol. 68, No. 8, 1316–1320, Feb. 2020.
6. Li, M., X. Chen, A. Zhang, and A. A. Kishk, "Dual-polarized broadband base station antenna backed with dielectric cavity for 5G communications," *IEEE Antennas and Wireless Propagation Letters*, Vol. 18, No. 10, 2051–2055, Oct. 2019.
7. Yang, S. J., Y. M. Pan, Y. Zhang, Y. Gao, and X. Y. Zhang, "Low-profile dual-polarized filtering magneto-electric dipole antenna for 5G applications," *IEEE Transactions on Antennas and Propagation*, Vol. 67, No. 10, 6235–6243, Oct. 2019.

8. Thi Cam Ha, L., S. X. Ta, N. X. Quyen, N. K. Kiem, and D. N. Chien, "Design of compact broadband dual-polarized antenna for 5G applications," *Int. J. RF Microw Comput. Aided Eng.*, Vol. 31, No. 5, e22615, 2021.
9. Zhang, Z. Y., Y. Zhao, D. Wu, S. L. Zuo, L. Ji, X D. Yang, and G. Fu, "Dual-polarised crossed-dipole antenna with improved beamwidth," *IET Microwaves, Antennas and Propagation*, Vol. 12, No. 6, 890–894, 2018.
10. Feng, B., C. Zhu, J. Cheng, C. Sim, and X. Wen, "A dual-wideband dual-polarized magneto-electric dipole antenna with dual wide beamdwidths for 5G MIMO microcell applications," *IEEE Access*, Vol. 7, 43346–43355, Apr. 2019.
11. Ta, S. X., C. D. Bui, and T. K. Nguyen, "Wideband quasi-Yagi antenna with broad-beam dual-polarized radiation for indoor access points," *Applied Computational Electromagnetics Society Journal*, Vol. 34, No. 5, 654–660, May 2019.
12. Yin, J. Y. and L. Zhang, "Design of a dual-polarized magnetoelectric dipole antenna with gain improvement at low elevation angle for a base station," *IEEE Antennas and Wireless Propagation Letters*, Vol. 19, No. 5, 756–760, May 2020.
13. He, Y. and Y. Li, "Dual-polarized microstrip antennas with capacitive via fence for wide beamwidth and high isolation," *IEEE Transactions on Antennas and Propagation*, Vol. 68, No. 7, 5095–5103, Jul. 2020.
14. Sabharwal, A., P. Schniter, D. Guo, D. W. Bliss, S. Rangarajan, and R. Wichman, "In-band full-duplex wireless: challenges and opportunities," *IEEE Journal on Selected Areas in Communications*, Vol. 32, No. 9, 1637–1651, Sep. 2014.
15. Debaillie, B., D. Broek, C. Lavin, B. Liempd, E. Klumperink, C. Palacios, J. Craninckx, B. Nauta, and A. Parssinen, "Analog/RF solutions enabling compact full-duplex radios," *IEEE Journal on Selected Areas in Communications*, Vol. 32, No. 9, 1662–1673, Sep. 2014.
16. Nawaz, H. and I. Tekin, "Double-differential-fed, dual-polarized patch antenna with 90 dB interport RF isolation for a 2.4 GHz in-band full-duplex transceiver," *IEEE Antennas and Wireless Propagation Letters*, Vol. 17, No. 2, 287–290, Feb. 2018.
17. Lin, X.-J., Z.-M. Xie, and P.-S. Zhang, "High isolation dual-polarized patch antenna with hybrid ring feeding," *International Journal of Antennas and Propagation*, Vol. 2017, Article ID: 6193102, May 2017.
18. Mirmozafari, M., G. Zhang, S. Saeedi and R. J. Doviak, "A dual linear polarization highly isolated crossed dipole antenna for MPAR application," *IEEE Antennas and Wireless Propagation Letters*, Vol. 16, 1879–1882, 2017.
19. Feng, B., X. He, J. Cheng, Q. Zeng, and C. Sim, "A low-profile differentially fed dual-polarized antenna with high gain and isolation for 5G microcell communications," *IEEE Transactions on Antennas and Propagation*, Vol. 68, No. 1, 90–99, Jan. 2020.
20. Ta, S. X., N. Nguyen-Trong, V. C. Nguyen, K. K. Nguyen, and D.-N. Chien, "Broadband dual-polarized antenna using metasurface for full-duplex applications," *IEEE Antennas and Wireless Propagation Letters*, Vol. 20, No. 2, 254–258, Feb. 2021.
21. Edward, B. and D. Rees, "Microstrip fed printed dipole with an integrated balun," US Patent 4 825 220, Nov. 26, 1986.
22. Zhang, Z.-Y., Y.-X. Guo, L. C. Ong, and M. Y. W. Chia, "A new wide-band planar balun on a single-layer PCB," *IEEE Microw. Wireless Compon. Lett.*, Vol. 15, No. 6, 41–418, Jun. 2005
23. Nawaz, H. and I. Tekin, "Dual-polarized, differential fed microstrip patch antennas with very high interport isolation for full-duplex communication," *IEEE Transactions on Antennas and Propagation*, Vol. 65, No. 12, 7355–7360, Dec. 2017.
24. Erol, L. Y., A. Uzun, M. Seyyedesfahlan, and I. Tekin, "Broadband full-duplex antenna for IEEE 802.11 protocols," *IEEE Antennas and Wireless Propagation Letters*, Vol. 20, No. 10, 1978–1982, Oct. 2021.